# The 4s ← 3p Electronic Transition in Aluminum Atom−Molecule Complexes: Bound and Repulsive Excited States

**Xiaofeng Tan and Paul J. Dagdigian***

*Department of Chemistry, The Johns Hopkins University, Baltimore, Maryland 21218-2685*

*Received: June 25, 2001; In Final Form: October 4, 2001*

An investigation of the 4s ← 3p electronic transition in weakly bound binary complexes of the Al atom with Ne and several molecules ($H_2$, $D_2$, $N_2$, $CH_4$) is reported. In contrast with the higher excited Al atomic states where the interactions are attractive, the observed spectra are indicative of both attractive and repulsive interactions of Al(4*s*) with these partners. No fluorescence was detected upon laser excitation of this electronic transition in the Al−$N_2$ and Al−$CH_4$ complexes. Fluorescence depletion spectroscopy, using the 3d ← 3p electronic transition as the probe transition, was employed to observe these transitions. The 4s ← 3p transitions in Al−$N_2$ and Al−$CH_4$ show vibrational structure, assigned as excited-state progressions in the van der Waals stretch mode. An unstructured feature to the blue of the Al 4s ← 3p atomic transition was observed in the laser fluorescence excitation spectra of the AlNe, Al−$H_2$, and Al−$D_2$ complexes. These spectra are a consequence of the repulsive nature of the interaction of Al(4s) with these partners, as in the corresponding isovalent complexes involving the boron 3s state. With the availability of an ab initio potential energy curve for the ground state, a potential energy curve for the excited AlNe($B\ ^2\Sigma^+$) electronic state was derived by a fit to the observed AlNe excitation spectrum.

## 1. Introduction

There has been considerable interest in the interaction of metal atoms, in both their ground and their electronically excited states, with small molecules. In part, this interest stems from a desire to relate properties, such as the electronic absorption spectra, of cryogenic solid hydrogen doped with these atoms[1−3] to the two-body atom-molecule interaction. An understanding of the structure and dynamics of atom-doped solid hydrogen is of both fundamental and potential technological interest. The nonbonding interactions between pairs of metal atoms and small molecules have been characterized through spectroscopic investigations of weakly bound complexes of these species. In our laboratory, we have employed laser fluorescence excitation (FE) and laser fluorescence depletion (FD) spectroscopy of weakly bound group 13 atoms with small molecules, involving boron[4,5] and aluminum[6−11] to probe these interactions.

In contrast to Al atom−rare gas diatomic complexes, which generally decay radiatively, the bound excited states of Al atom−small molecule complexes which have thus far been studied all appear to predissociate. This makes it difficult to study the electronic spectrum of these complexes. One approach to circumvent the problem of predissociation is to excite the Al atom−molecule complexes to higher electronic states and then observe emission from the low-lying excited Al atomic levels formed by the predissociation. We have used this type of action spectroscopy to characterize the 5s ← 3p and 4d ← 3p transitions of the Al−$H_2$, Al−$N_2$, and Al−$CH_4$ complexes.[6−8] Other approaches that have been applied to the study of Al atom−molecule complexes include 1-photon photoionization,[12] resonance-enhanced multiphoton ionization (REMPI),[13,14] and zero electron kinetic energy (ZEKE)[15,16] spectroscopy. Laser fluorescence excitation has also been employed in the study of the isovalent Ga−$N_2$ complex.[17] A laser fluorescence spectroscopic study of the solvation of Al atoms in superfluid helium droplets has also been carried out.[18]

In recent work, we have characterized the 3d, 4p, 4d ← 3p transitions in the Al−$H_2$ and Al−$D_2$ complexes through laser fluorescence excitation and laser fluorescence depletion spectroscopies.[9] A collaborative experimental and theoretical investigation of the rotational structure of the Al(3p)−$H_2/D_2$ complex has been conducted in conjunction with Alexander and Williams.[10] Rotational constants and parity splitting parameters determined in the experiment were found to be in very good agreement with the theoretical values derived from the new Al(3p)−$H_2$ potential energy surfaces (PESs), for which the $H_2$ vibrational motion was explicitly taken into account. Together with our previous work on the 5s ← 3p and 4d ← 3p transitions of the Al−$H_2$, Al−$N_2$, and Al−$CH_4$ complexes,[6−8] considerable information about the nonbonding interactions of the ground 3p and low-lying Rydberg electronic states of the Al atom with various small molecule complexes has been obtained. In previous work, we have also observed transitions to bound electronic states of the AlNe complex correlating with the 3d and 5s atomic states.[19]

In contrast with transitions to the higher Rydberg states in Al atom−molecule complexes, the 4s ← 3p transition, involving the lowest electronic transition in the Al atom, has not been previously investigated. In an extension of our earlier investigations, we have carried out an experimental study of this transition in the Al−$H_2/D_2$, Al−$N_2$, Al−$CH_4$, and AlNe complexes. In this paper, we present a FD study of this transition for the Al−$N_2$ and Al−$CH_4$ complexes and a FE study of the same transition in the AlNe, Al−$H_2$, and Al−$D_2$ complexes. We also report here the observation of the 3d ← 3p transition in the Al−$N_2$ and Al−$CH_4$ complexes, which were used as the probe transitions in the FD experiments. The FD technique, which is a folded variant of optical−optical double resonance spectroscopy, allows the study of transitions for which the excited state does not radiatively decay. This technique has been applied

10.1021/jp0123987 CCC: $20.00 
Published on Web 11/16/2001

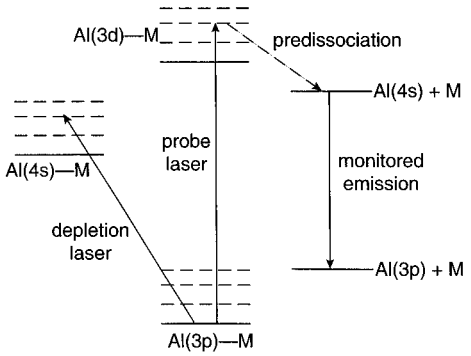


**Figure 1.** Schematic diagram of the technique of fluorescence depletion as applied to the Al−$N_2$ and Al−$CH_4$ complexes. The depletion laser was scanned through the 4s ← 3p transition in the complex while the probe laser was tuned to a 3d ← 3p band of the complex. The depletion signal was monitored by observing aluminum atom 4s → 3p emission.

previously to the study of transitions in van der Waals complexes.[20−23]

We find from the present study that the nonbonding interaction of the Al(4s) atom with small molecules can be both attractive and repulsive, depending on the ligand. In contrast to our observations for the Al−$N_2$ and Al−$CH_4$ complexes, an emission signal is observed to the blue of the Al 4s ← 3p atomic transition upon excitation of this transition in the AlNe and Al−$H_2$/$D_2$ complexes. This indicates that the AlNe and Al−$H_2$/$D_2$ 4s electronic states are repulsive in the Franck−Condon region. These results are entirely analogous with the corresponding 3s ← 2p transition in the isovalent BNe and B−$H_2$/$D_2$ complexes, which were previously studied in our laboratory.[4,24]

## 2. Experimental Section

The Al atom−molecule van der Waals complexes were formed in a pulsed free jet expansion. The apparatus in which the present experiment was carried out has been described in detail previously.[7,24,23] In brief, a supersonic beam containing aluminum atoms and the desired Al atom−molecule complex was produced in a pulsed free jet expansion (0.2 mm diameter orifice) of mixtures of trimethylaluminum (TMA, obtained from Aldrich Chemical Co.), the desired ligand ($N_2$, $CH_4$, $H_2$, $D_2$, or Ne) and helium through 193 nm photolysis of TMA at the nozzle orifice. The laser excitation zone for both FE and FD spectra was 1.2 cm downstream of the nozzle.

Figure 1 presents a schematic diagram for the FD setup. The 4s ← 3p transition in the complex was excited by the depletion laser, and the 3d ← 3p transition was used to probe the depletion. In practice, the depletion laser was scanned through the 4s ← 3p transition region, whereas the probe laser was fixed to the center of a strong band of the 3d ← 3p transition and fired after the depletion laser. Emission from the Al 4s atoms, which were formed by predissociation of the Al(3d)−M complex, was detected with a photomultiplier (Thorn EMI 9813QB). Each time the depletion laser was resonant with a transition in the Al(4s)−M complex, the population of the ground-state complex decreased and the monitored atomic emission dropped.

FE spectra were recorded using frequency-doubled signal output of a Continuum Powerlite Precision 8000 Nd:YAG pumped Sunlite EX BBO optical parametric oscillator (OPO). The bandwidth of the UV radiation was ∼0.2 $cm^{-1}$, and the typical pulse energy of the 0.3 cm diam beam entering the beam apparatus was 20−40 $\mu$J. In the FD experiments, frequency-doubled output of a Nd:YAG laser pumped dye laser (Continuum ND6000) was used as the probe laser. The output from the OPO was used as the depletion laser and spatially overlapped with the probe laser beam. The depletion laser beam diameter was twice as that of the probe laser. The depletion laser was fired 110−220 ns before the probe laser. Typical pulse energies of the depletion and probe lasers were 250 $\mu$J and 50 $\mu$J, respectively. The depletion laser was fired on every other molecular beam pulse, and the probe-laser-induced fluorescence signals were separately summed for the depletion laser on and off over a preset number of shots (typically 10) before the depletion laser was stepped to the next wavelength.

In both FE and FD experiments, the laser wavenumber was calibrated using the Al 4s $^2S_{1/2}$ ← 3p $^2P_{1/2,3/2}$ atomic lines and a solid fused-silica etalon (free spectral range 0.676 $cm^{-1}$ in the visible).

## 3. Results

**3.1. Al−$N_2$ and Al−$CH_4$ Complexes.** When the excitation laser was scanned ± 800 $cm^{-1}$ from the Al 4s ← 3p atomic transition, neither resonance fluorescence from Al(4s)−$N_2$ or Al(4s)−$CH_4$ nor Al 4s → 3p atomic emission was observed. This suggests that the excited Al(4s)−$N_2$ and Al(4s)−$CH_4$ complexes do not decay radiatively. Predissociation likely occurs through coupling with a repulsive PES emanating from the ground Al(3p) asymptote. As illustrated by ab initio calculations on the Al−$NH_3$ complex,[13] this state is the analogue of the $A^2\Sigma^+$ state of a diatomic Al atom−rare gas complex.

Previous work[7,8] showed that the Al−$N_2$ and Al−$CH_4$ complexes can be formed in our supersonic beam expansions. The fluorescence depletion scheme was then employed to observe these electronic transitions. In this section, we report our observations of both the 3d ← 3p and 4s ← 3p transitions in these complexes. The former transition could be observed by fluorescence excitation spectroscopy. These were used as the probe transitions in order to detect the 4s ← 3p transition in these complexes.

*3.1.1. 3d ← 3p Transition.* The 3d ← 3p transitions in the Al−$N_2$ and Al−$CH_4$ complexes were observed by monitoring 4s → 3p emission from Al(4s) atoms produced by predissociation of the excited complexes, whereas the excitation laser was scanned through the spectral region of the 3d ← 3p atomic transition. The assignment of these features to the Al−$N_2$ and Al−$CH_4$ complexes is straightforward since the beam conditions were quite similar to those previously employed to observe the 5s, 4d ← 3p transitions in these complexes.[7,8]

Figure 2 presents a typical FE spectrum for the 3d ← 3p transition in the Al−$N_2$ complex. Excitation spectra with the same intensity distribution among the bands was observed for $N_2$ mole fractions ranging from 2 to 20%. These spectral features disappeared when $N_2$ was removed from the seed gas mixture. Moreover, the bands were seen only when TMA was present in the seed gas and the photolysis laser was on. We thus assign these features to the Al−$N_2$ complex. As noted in the caption of Figure 2, excitation spectra were recorded with a small amount of Ar added to the $N_2$/He seed gas mixtures. We found that without Ar present the Al−$N_2$ bands could not be observed. In our previous spectroscopic study of the Al−$N_2$ complex,[7] the seed gas was usually a $N_2$/Ar mixture. Our present observations suggest that the formation of Al−$N_2$ in the supersonic beam is greatly facilitated by the formation of AlAr and the subsequent formation of Al−$N_2$ by the exchange process

$$\mathrm{AlAr} + \mathrm{N_2} \rightarrow \mathrm{Al{-}N_2} + \mathrm{Ar}. \qquad (1)$$

This reaction is exothermic since the binding energy of Al−$N_2$ is greater than that of AlAr.[7]

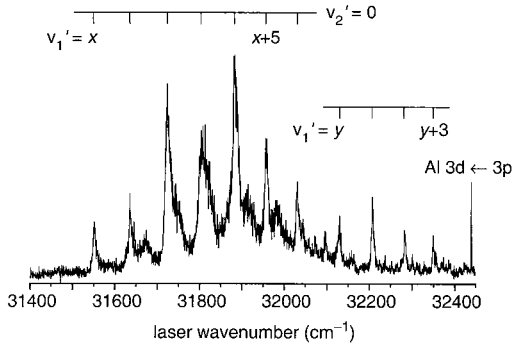


**Figure 2.** Survey scan of the FE spectrum of the 3d ← 3p transition in the Al−$N_2$ complex. Al atomic 4s → 3p emission at 395 nm was monitored while the excitation laser wavenumber was scanned. The Al 3d $^2D_J$−3p $^2P_{1/2}$ atomic line is indicated in the figure, as are several excited-state progressions of the van der Waals stretch mode in the Al(3d)−$N_2$ complex (see text). The beam seed gas mixture was 5% $N_2$, 2% Ar, and 93% He, at a total backing pressure of 15 atm.

The spectrum displayed in Figure 2 shows banded structure to the red of the Al 3d ← 3p atomic transition, reflecting the attractive nature of the interaction of the electronically excited Al(3d) atom with molecular nitrogen. The spectrum appears more congested than those for the 5s ← 3p and 4d ← 3p transitions, which were dominated by a single excited-state progression in the Al−$N_2$ van der Waals stretch vibrational mode.[7] Two strong progressions starting near 31 550 and 32 120 $cm^{-1}$ can be seen in the spectrum displayed in Figure 2. The wavenumber spacings of bands within a progression are consistent with the vibrational frequency of the Al−$N_2$ stretch vibration and are assigned as such. In addition to these identified progressions, there are a number of weaker bands which appear in the same wavenumber range as the progression starting at 31 550 $cm^{-1}$. We also scanned to the red of the spectral region displayed in Figure 2 and found a weak, but unstructured, signal assignable to Al−$N_2$ extending more than 1700 $cm^{-1}$ to the red of the Al 3d ← 3p atomic transition. No definitive spectral assignment of this signal could be made.

The equilibrium geometry of the ground $^2\Pi$ electronic state of the Al−$N_2$ complex, which correlates with the Al(3p) + $N_2$ asymptote, is linear.[7,25] The bending frequency is estimated[25] to be 56 $cm^{-1}$, which suggests little population of excited bending levels in the beam. Moreover, the equilibrium geometry of the $Al^+$−$N_2$ ionic complex is also computed to be linear.[25] This geometry is consistent with the known negative sign of the $N_2$ electric quadrupole moment[26] and the angular dependence of the ion-quadrupole interaction.[27] In view of the fact that the ground states of the neutral and ionic Al−$N_2$ complexes both have linear geometries, we expect that the Rydberg states would also be linear.

In linear geometry, there are three Al−$N_2$ electronic states, $^2\Delta$, $^2\Pi$, and $^2\Sigma^+$, associated with the asymptotic Al(3d) atomic state. In analogy with the Rydberg states of Al−rare gas diatomic complexes, as exemplified by AlAr,[28] the binding energies should fall in the order $^2\Delta > {}^2\Pi > {}^2\Sigma^+$, to minimize the Pauli repulsion of the singly occupied Al atomic orbital with molecular electron cloud. The two observed progressions in the 3d ← 3p transition of the Al−$N_2$ complex are assigned as excitation of van der Waals stretch vibrational levels in the excited $^2\Delta$ and $^2\Pi$ electronic states. No assignments have been made for the weaker bands.

Table 1 presents the transition wavenumbers for the bands assigned to progressions in the van der Waals stretch vibrational mode in the excited Al−$N_2$ $^2\Delta$ and $^2\Pi$ electronic states. The transition wavenumbers of the bands were estimated as the wavenumber of the maximum intensity within each band. It was not possible to assign unambiguously the transition in each progression to the lowest stretch level $v_s' = 0$, where $v_s'$ denotes the van der Waals stretch quantum number. Accordingly, we have given arbitrary designations of the stretch quantum numbers $v_s'$ for which the lowest vibrational quantum numbers have been assigned to $x$ ($x \geq 0$) and $y$ ($\geq 0$) for the progressions to the $^2\Delta$ and $^2\Pi$ electronic states, respectively.

**TABLE 1: Band Positions (in $cm^{-1}$) for Transitions to van der Waals Stretch Vibrational Levels of Al(3d)−$N_2$ Electronic States[a]**

| $v_s'$ | transition wavenumber |
|---|---|
| $^2\Delta$ electronic state | |
| $x$[b] | 31 547.8(2) |
| $x+1$ | 31 632.9(3) |
| $x+2$ | 31 719.7(2) |
| $x+3$ | 31 799.6(5) |
| $x+4$ | 31 880.9(2) |
| $x+5$ | 31 953.9(2) |
| $x+6$ | 32 027.1(2) |
| $^2\Pi$ electronic state | |
| $y$ | 32 125.0(3) |
| $y+1$ | 32 203.7(1) |
| $y+2$ | 32 279.0(1) |
| $y+3$ | 32 345.4(2) |

[a] Standard deviation of the band positions are given in parentheses in units of the last significant digit. [b] Vibrational assignment is not certain; see text.

The bands displayed in Figure 2 are fairly broad, and the rotational structure could not be resolved. This contrasts with the 5s ← 3p transition, for which the Lorentzian width was sufficiently narrow that the bands could be partially resolved.[7] The profiles of the bands in Figure 2 cannot be fitted to pure Lorentzian profiles. There appears to be a significant heterogeneous component to the width, due to the rotational structure, within each band. The band contours were compared with Lorentzian profiles to estimate an upper bound to the width of a Lorentzian profile which can be embedded within the contour. For the transitions to the excited $^2\Delta$ and $^2\Pi$ electronic states, we estimate upper bounds to the Lorentzian widths of $\leq 20$ and $\leq 9$ $cm^{-1}$, respectively, implying excited-state predissociation lifetimes of $\geq 0.12$ and $\geq 0.3$ ps.

The transition wavenumbers $T_v$ reported in Table 1 were employed to determine vibrational constants for the Al(3d)−$N_2$ electronic states. Expressing the excited-state vibrational energy as a quadratic in the van der Waals stretch vibration quantum number $v_s'$, we write

$$T_v = T_{00} + \omega_e' v_s' - \omega_e x_e' v_s' (v_s' + 1) \qquad (2)$$

For the pure stretch progression in the $^2\Delta$ electronic state, we obtain the following spectroscopic constants with the assumption that $x = 0$: $T_{00} = 31\,456.4 \pm 2.3$, $\omega_e' = 93.5 \pm 1.5$, $\omega_e x_e' = 1.50 \pm 0.16$ $cm^{-1}$. We obtain the following constants for the pure stretch progression in the $^2\Pi$ electronic state with the assumption that $y = 0$: $T_{00} = 32\,124.7 \pm 1.2$, $\omega_e' = 86.0 \pm 2.5$, $\omega_e x_e' = 3.08 \pm 0.61$ $cm^{-1}$.

The dissociation energy of the ground 3p state of the Al−$N_2$ complex has previously been estimated to equal $300 \pm 50$ $cm^{-1}$.[7] This value is consistent with earlier experimental and theoretical estimates.[12,25] With this value and the observed transition wavenumbers, lower bounds to the excited-state dissociation energies can be obtained. We estimate $D_0' \geq 1190$ and 610 $cm^{-1}$ for the assigned $^2\Delta$ and $^2\Pi$ electronic states, respectively, both with uncertainties of $\pm 50$ $cm^{-1}$.

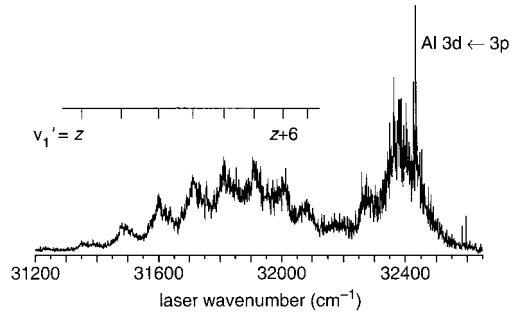


**Figure 3.** Survey scan of the FE spectrum of the 3d ← 3p transition in the Al−$CH_4$ complex. Al atomic 4s → 3p emission at 395 nm was monitored while the excitation laser wavenumber was scanned. The Al 3d $^2D_J$−3p $^2P_{1/2}$ atomic line is indicated in the figure, as is an excited-state progression of the van der Waals stretch mode in the Al(3d)−$CH_4$ complex (see text). The beam seed gas mixture was 20% $CH_4$ and 80% He, at a total backing pressure of 17 atm.

**TABLE 2: Band Positions (in cm$^{-1}$) for Transitions to van der Waals Stretch Excited Levels of Al(3d)-$CH_4$[a]**

| $v_s'$ | transition wavenumber |
|---|---|
| $z$[b] | 31 356.7(15) |
| $z+1$ | 31 493.1(11) |
| $z+2$ | 31 608.9(14) |
| $z+3$ | 31 716.6(11) |
| $z+4$ | 31 818.8(15) |
| $z+5$ | 31 912.2(16) |
| $z+6$ | 32 005.5(16) |
| $z+7$ | 32 077.0(16) |

[a] Standard deviation of the band positions are given in parentheses in units of the last significant digit. [b] Vibrational assignment is not certain; see text.

Figure 3 presents an FE scan of the 3d ← 3p transition in the Al−$CH_4$ complex. As was the case for Al−$N_2$, for this transition, no resonance fluorescence was detected, and the transition was observed by monitoring Al 4s → 3p atomic emission as the laser wavenumber was scanned. Two groups of bands are apparent in the spectrum. The lower wavenumber set of bands appears to form an excited-state van der Waals stretch progression. It is not possible to assign unambiguously the first member of this progression, and we assign the vibrational quantum number of the first observed band as $v_s' = z$, where $z \geq 0$. The second group of bands, around 32 400 cm$^{-1}$, does not follow the intensity distribution in this progression and appears to belong to a different transition.

Table 2 presents the transition wavenumbers for the lower-energy bands, estimated from the maximum intensity within each band. We obtain the following spectroscopic constants from a fit of the transition wavenumbers to eqn 1 with the assumption that $z = 0$: $T_{00} = 31\,360.2 \pm 3.6$, $\omega_e' = 136.1 \pm 2.5$, $\omega_e x_e' = 4.20 \pm 0.31$ cm$^{-1}$. The vibrational structure is not well resolved in the higher-energy transition displayed in Figure 3 for the Al−$CH_4$ complex. The widths of the bands in this progression are significantly greater than of those of the previously reported Al(5s)−$CH_4$ and Al(4d)−$CH_4$ bands.[8] The band contours cannot be fitted to pure Lorentzian profiles. An upper bound to the Lorentzian width, $\leq 80$ cm$^{-1}$, was estimated in the same manner as described previously and corresponds to an excited-state lifetime of $\geq 0.03$ ps.

To our knowledge, the nonbonding interaction of the Al(3p) atom with $CH_4$ has not been investigated by quantum chemical calculations. In the likely $C_{3v}$ geometry of the ground electronic state (ignoring Jahn−Teller distortions), the Al 3d atomic state will split into three electronic states ($A_1 + 2E$), in analogy to the Al−$N_2$ electronic states. It is reasonable to assign the two observed groups of bands as excitation to two of these states, similar to the assignment of the Al−$N_2$ bands.

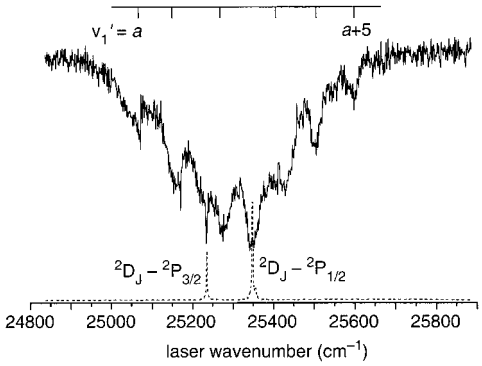


**Figure 4.** Fluorescence depletion spectrum of the 4s ← 3p transition in the Al−$N_2$ complex (solid line). The probe laser was tuned to excite the $v_s' = x + 3$ band of the 3d ← 3p transition in the $^2\Delta$ electronic state, while emission in the Al 4s → 3p transition was monitored. The depletion laser power density was 20 $\mu$J/mm$^2$ and fired 200 ns before the probe laser; the probe laser power density was 9 $\mu$J/mm$^2$. For the strongest band in the spectrum, the FD signal corresponds to 50% depletion of the probe laser induced fluorescence signal. The beam seed gas mixture was 5% $N_2$, 2% Ar, and 93% He, at a total backing pressure of 13 atm. The dotted trace represents a laser fluorescence excitation spectrum of atomic Al. The 3d $^2D_J$ − 3p $^2P_{1/2,3/2}$ atomic lines are indicated in the figure, as is an assigned excited-state progression of the van der Waals stretch mode in the Al(4s)−$N_2$ complex. The FD signals at the Al atomic lines are artifacts (see text).

*3.1.2. The 4s ← 3p Transition.* As discussed above, no resonance fluorescence was observed for the Al−$N_2$ and Al−$CH_4$ complexes when the spectral region of the 4s ← 3p transition was scanned. With the FD technique, the 4s ← 3p transition was found for both complexes. In both cases, one of the bands in the 3d ← 3p transition was employed as the probe transition in the FD experiment.

Figure 4 presents the FD spectrum for the Al−$N_2$ complex. A progression of broad bands was observed. For reference, a fluorescence excitation spectrum of atomic Al is superimposed to illustrate the displacement of the Al−$N_2$ bands from the wavenumbers of the Al 4s $^2S_{1/2}$ ← 3p $^2P_{1/2,3/2}$ atomic lines. It can be seen that the progression extends through the region of the atomic transition. Two features in the FD spectrum appear at the transition wavenumbers of the atomic lines. These are spurious and result from saturation effects caused by the strong 4s → 3p fluorescence excited by the depletion laser as it is scanned through the atomic lines. The artifact at the $^2S_{1/2}$ ← $^2P_{1/2}$ atomic line is broader because of the greater intensity of the line in the FE spectrum involving excitation from the ground atomic level.

The observed bands in Figure 4 appear to form an excited-state progression in the van der Waals stretch vibrational mode, as in the other electronic transitions. It was not possible to assign unambiguously the transition to the lowest excited stretch level $v_s' = 0$. We have thus given arbitrary designations for the stretch quantum numbers $v_s'$, as was done for the other observed progressions and have set $v_s' = a$ ($a \geq 0$) for the lowest-energy observed band. Table 3 gives the transition wavenumbers of the bands, estimated as the wavenumber corresponding to the maximum intensity of the band. The spacings between the bands are not monotonic. This probably reflects the varying displacements of the wavenumber of maximum intensity from that of the band origin as a function of $v_s'$ and the distortion of the $v_s' = a + 3$ band because of the saturation at the Al 4s $^2S_{1/2}$ ← 3p $^2P_{1/2}$ atomic line.

**TABLE 3: Band Positions (in cm$^{-1}$) for Transitions to van der Waals Stretch Excited Levels of Al(4s)-$N_2$[a]**

| $v_s'$ | transition wavenumber |
|---|---|
| $a$[b] | 25 061.9(26) |
| $a+1$ | 25 161.4(8) |
| $a+2$ | 25 276.2(8) |
| $a+3$ | 25 400[c] |
| $a+4$ | 25 504.2(5) |
| $a+5$ | 25 596.4(10) |

[a] Standard deviation of the band positions are given in parentheses in units of the last significant digit. [b] Vibrational assignment is not certain; see text. [c] Estimated transition wavenumber; band is very close to a strong atomic line (see text).

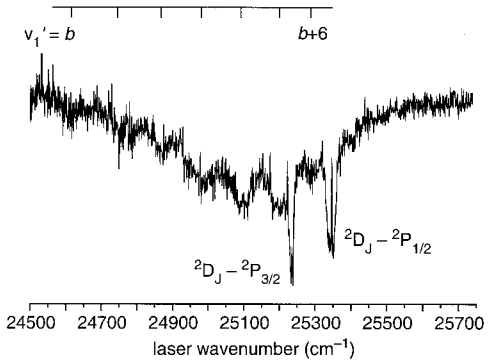


**Figure 5.** Fluorescence depletion spectrum of the 4s ← 3p transition in the Al−$CH_4$ complex. The probe laser was tuned to excite the $v_s' = z + 4$ band of the 3d ← 3p transition, while emission in the Al 4s → 3p transition was monitored. The depletion laser power density was 18 $\mu$J/mm$^2$ and fired 110 ns before the probe laser; the probe laser power density was 8 $\mu$J/mm$^2$. For the strongest band in the spectrum, the FD signal corresponds to 50% depletion of the probe laser induced fluorescence signal. The beam seed gas mixture was 20% $CH_4$ and 80% He, at a total backing pressure of 17 atm. The 3d $^2D_J$−3p $^2P_{1/2,3/2}$ atomic lines are indicated in the figure, as is an assigned excited-state progression of the van der Waals stretch mode in the Al(4s)−$N_2$ complex. The FD signals at the Al atomic lines are artifacts (see text).

Because of the nonmonotonic spacings between the bands, a fit of the band positions to eq 1 was not carried out. From the spacings between the bands, a vibrational frequency $\omega_e' \approx 118$ cm$^{-1}$ was estimated with the assumption that $a = 0$. We obtain a lower bound to the binding energy in the excited state of $D_0' \geq 583 \pm 50$ cm$^{-1}$. Upper bounds to the Lorentzian widths of the bands, estimated as described previously, are $\leq$35 cm$^{-1}$.

Figure 5 presents a FD spectrum for the 4s ← 3p transition in the Al−$CH_4$ complex. Again, spurious signals appear at the wavenumbers of the Al atomic lines because of saturation effects associated with the strong atomic fluorescence excited at these depletion laser wavenumbers. The signal-to-noise ratio in this spectrum is not as good as in the Al−$N_2$ spectrum displayed in Figure 4. However, a single progression can be identified and assigned as a progression in the excited-state van der Waals stretch vibrational mode. It was again not possible to assign unambiguously the transition to the lowest excited stretch level $v_s' = 0$, and the lowest-energy band is assigned $v_s' = b$ ($b \geq 0$). Table 4 lists the transition wavenumbers, estimated as the wavenumber corresponding to the maximum intensity in the band. Setting $D_0''$(Al−$CH_4$) = 400 cm$^{-1}$ as before,[8] we can estimate a lower bound to the excited-state binding energy, $D_0' \geq 1131$ cm$^{-1}$. From the spacings between the bands, a vibrational frequency $\omega_e' \approx 140$ cm$^{-1}$ was estimated with the assumption that $b = 0$. Upper bounds to the Lorentzian widths of the bands, estimated as described previously, are $\leq$ 55 cm$^{-1}$.

**3.2. 4s ← 3p Transition in AlNe, Al−$H_2$, and Al−$D_2$.** This electronic transition in the AlNe, Al−$H_2$, and Al−$D_2$ complexes has a qualitatively different appearance than for the corresponding transition in the Al−$N_2$ and Al−$CH_4$ complexes. In all cases, a broad structureless feature was observed in the fluorescence spectra to the blue of the Al 4s ← 3p atomic transition whereas excitation laser was scanned through the 4s ← 3p transition in the complexes and the Al 4s → 3p atomic emission was monitored. Within the spectral resolution of the detection monochromator, the observed emission appears to be at the wavenumber of the atomic transition.

**TABLE 4: Band Positions (in cm$^{-1}$) for Transitions to van der Waals Stretch Excited Levels of Al(4s)-$CH_4$[a]**

| $v_s'$ | transition wavenumber |
|---|---|
| $b$[b] | 24 617.7(43) |
| $b+1$ | 24 753.3(21) |
| $b+2$ | 24 874.1(17) |
| $b+3$ | 24 993.4(23) |
| $b+4$ | 25 098.5(14) |
| $b+5$ | 25 200.3(18) |
| $b+6$ | 25 293.2(22) |

[a] Standard deviation of the band positions are given in parentheses in units of the last significant digit. [b] Vibrational assignment is not certain; see text.

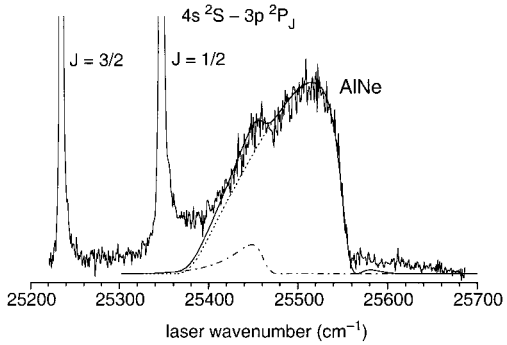


**Figure 6.** Laser fluorescence excitation spectrum of the 4s ← 3p transition in the AlNe complex. The solid line with noise is the recorded experimental spectrum. Al atomic 4s → 3p emission at 395 nm was monitored whereas the excitation laser wavenumber was scanned. The beam seed gas mixturs was 15% Ne and 85% He, at a backing pressure of 18 atm. The experimental spectrum is compared with a simulated spectrum (smooth solid curve) derived from the ab initio potential energy curve of the $X\ ^2\Pi$ state (ref [19]) and manually fit $B\ ^2\Sigma^+$ state potential energy curve. The dotted curve is the simulated spectrum for excitation out of the ground $X_1\ ^2\Pi_{1/2}$ spin−orbit manifold, whereas the dot−dashed curve is a simulation (scaled by multiplication by the factor 0.07) for excitation out of the spin−orbit excited $X_2\ ^2\Pi_{3/2}$ manifold. The smooth solid curve is the sum of the simulations for excitation of the two $X\ ^2\Pi$ spin−orbit manifolds.

*3.2.1. AlNe Complex.* Figure 6 presents a scan of the laser fluorescence excitation spectrum of a free jet containing Al atoms and the AlNe complex. In addition to the Al 4s $^2S_{1/2}$ ← 3p $^2P_{1/2,3/2}$ atomic lines, a broad, unstructured feature which has its maximum intensity approximately 170 cm$^{-1}$ to the blue of the $^2S_{1/2}$ ← $^2P_{1/2}$ atomic line. As indicated by the signal-to-noise ratio in the spectrum, the intensity of the observed feature is quite weak. We assign this feature to the AlNe complex for the following reasons: This spectral feature is present in the FE spectrum only when Ne is present in the beam seed gas mixture and is absent for a pure He seed gas; photolyzed TMA must also be present. The shape of this spectral feature was essentially unchanged for Ne mole fractions ranging from to 7 to 35%. Finally, the beam conditions were similar to those employed for the observation of the rotationally resolved 3d, 5s ← 3p bands in AlNe.[19]

This spectrum bears a striking resemblance to that of the free ← bound 3s ← 2p transition in the isovalent BNe complex.[24]

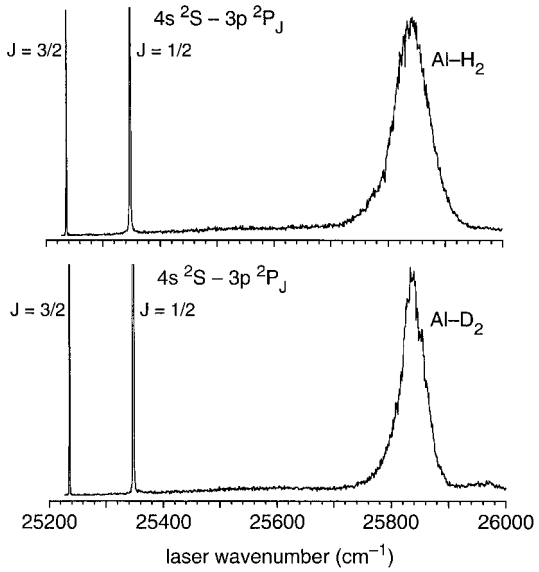


**Figure 7.** Laser fluorescence excitation spectrum of the 4s ← 3p transition in the Al−$H_2$ (top) and Al−$D_2$ (bottom) complexes. Al atomic 4s → 3p emission at 395 nm was monitored while the excitation laser wavenumber was scanned. The beam seed gas mixtures were 20% $H_2$ (for Al−$H_2$) or 20% $D_2$ (for Al−$D_2$) and 80% He, at backing pressures of 19 atm. The Al 4s $^2$S−3p $^2P_{1/2,3/2}$ atomic lines are identified. The unstructured features to the blue of the atomic lines are assigned to the Al−$H_2$ and Al−$D_2$ complexes.

As in the case of the BNe transition, the spectral feature has a markedly asymmetric profile, with the intensity falling off rapidly on the blue edge. There is also a subsidiary maximum on the shoulder of the profile ~60 cm$^{-1}$ to the red of the peak; this was reproducibly seen on all our recorded spectra. The unstructured nature of this transition, lying to the blue of the Al atomic transition, and our observation of the resulting emission near the wavelength of the atomic transition strongly suggest that the excited AlNe($B\ ^2\Sigma^+$) electronic state, which correlates with the Al(4s) + Ne asymptote, is repulsive. The observed emission is thus a result of dissociation in the excited electronic state

$$\mathrm{AlNe}(B\ ^2\Sigma^+) \rightarrow \mathrm{Al}(4s) + \mathrm{Ne}, \qquad (3)$$

followed by 4s → 3p fluorescence emission from the excited atom. Because the maximum in the AlNe FE spectrum lies approximately 170 cm$^{-1}$ to the blue of the $^2S_{1/2} \rightarrow {}^2P_{1/2}$ atomic transition, the AlNe($B\ ^2\Sigma^+$) potential energy curve can be estimated from the Franck−Condon principle[29,30] to be repulsive by roughly this magnitude (less the ground-state binding energy) at the equilibrium internuclear separation of the ground AlNe($X\ ^2\Pi_{1/2}$) electronic state.

A computed potential energy curve for the ground AlNe($X\ ^2\Pi_{1/2}$) spin−orbit manifold which has been calibrated by comparison with an experimentally determined dissociation energy $D_0$ is available.[19] It is possible then to derive a potential energy curve describing the excited AlNe($B\ ^2\Sigma^+$) electronic state by comparison of the experimentally observed AlNe spectrum with simulated spectra. The details of this procedure and the resulting potential energy curve are presented in Section 4.

*3.2.2. Al−$H_2$ and Al−$D_2$ Complexes.* When a photolyzed TMA/$H_2$/He gas mixture was expanded in the free jet, a broad, unstructured feature appeared in the laser fluorescence excitation spectrum. The top panel of Figure 7 shows a typical spectrum. The maximum intensity of this broad feature lies approximately 490 cm$^{-1}$ to the blue of the Al 4s $^2S_{1/2}$ ← 3p $^2P_{1/2}$ atomic line. Similarly, a broad feature was observed for beams containing photolyzed TMA/$D_2$/He gas mixtures, as illustrated by the spectrum displayed in the bottom panel of Figure 7. It should be noted that the width of the feature is slightly smaller with $D_2$ in the seed gas mixture than for $H_2$. These features are qualitatively similar to the analogous transition in AlNe, displayed in Figure 6, but the blue shifts are somewhat greater.

These broad spectral features can be straightforwardly assigned to the Al−$H_2$ and Al−$D_2$ complexes. The features are present in the FE spectra only when $H_2$ or $D_2$ are present in the seed gas mixture and are absent for a pure He seed gas. The shapes of this spectral features were essentially unchanged for $H_2$/$D_2$ mole fractions ranging from to 20 to 80%. Moreover, the beam conditions were similar to those employed for the observation of bands, in some cases rotationally resolved,[10] associated with transitions to higher electronic states in these complexes.[6,9]

As in the case of AlNe, discussed in the previous subsection, these transitions in Al−$H_2$ and Al−$D_2$ are assigned as free ← bound transitions in these complexes associated with the Al 4s ← 3p atomic transition, for which the excited-state PES is repulsive in the Franck−Condon region. The excitation energy of the Al(4s)−$H_2$/$D_2$ electronic state is sufficient to allow chemical reaction within the excited complexes to occur and form AlH/AlD($X^1\Sigma^+$) + H products.[6] Observation of these nonemitting products by laser fluorescence excitation above the large concentration of AlH/AlD in the beam[31] is probably not feasible. The repulsive nature of the Al(4s)−$H_2$ PES makes it unlikely that chemical reaction can occur before the atom−molecule pair dissociates on the excited PES.

From the blue shift of the maximum intensity of the spectral features from the Al 4s $^2S_{1/2}$ ← 3p $^2P_{1/2}$ atomic line, the repulsive energy of the Al(4s) + $H_2$ near the equilibrium geometry of the ground Al(3p)−$H_2$ PES can be estimated. Both of the Al−$H_2$ and Al−$D_2$ isotopomers can exist in two nuclear spin modifications. As discussed previously,[32,10] the dissociation energies of the Al(3p)−$o$$H_2$ and Al(3p)−$p$$D_2$ complexes, which are associated with the $j = 1$ diatom rotational levels, are significantly greater than for Al(3p)−$p$$H_2$ and Al(3p)−$o$$D_2$ ($j = 0$), respectively. The greater binding energies of the complexes involving $j = 1$ diatoms arises from the ability of the $j = 1$ diatom to align itself to sample preferentially the T-shaped equilibrium geometry, unlike the $j = 0$ diatom. Because of the greater binding energies of the nuclear spin modifications involving odd-$j$ diatom rotor levels, these are preferentially formed in the supersonic beam, as was verified in the spectroscopic analysis[10] of rotationally resolved bands.

The dissociation energies of the Al(3p)−$o$$H_2$/$p$$D_2$ complexes have been calculated using Al(3p)−$H_2$ PESs based on multireference configuration interaction calculations with an extrapolation to the complete basis set and an explicit inclusion of the dependence on the diatom bond distance.[32,10] The following values were obtained: $D_0 = 94.2$ and 112.0 cm$^{-1}$ for Al(3p)−$o$$H_2$ and Al(3p)−$p$$D_2$, respectively. Ignoring the angular dependence of the PES, this implies that the Al(4s)−$H_2$ PES has an energy of approximately 390 cm$^{-1}$ greater than that of the atom + diatom asymptote at the ground-state equilibrium geometry [Al−$H_2$ separation $R = 5.80$ bohr]. The dependence of the Al(4s)−$H_2$ interaction upon the atom−diatom separation $R$ has been computed for T-shaped geometry ($C_{2v}$ approach).[9] These calculations predict that the Al(4s)−$H_2$ PES for this geometry and $R = 5.8$ bohr has an energy approximately 280 cm$^{-1}$ higher than that of the Al(4s) +$H_2$ asymptote. Given the qualitative nature of this comparison, we conclude that the

calculations provide a reasonable description of the Al−$H_2$ interaction for this electronic state.

If the full angular and radial dependence of the excited-state Al(4s)−$H_2$ PES were available, then it would be possible to compare the experimental free ← bound excitation spectra with theoretical simulations in order to gain further information about the excited-state PESs. Such simulations were carried out in the case of the analogous 3s ← 2p transition in the B−$H_2$/$D_2$ complexes.[4]

We noted that the width of the spectral feature for Al−$D_2$ in Figure 7 is narrower than for Al−$H_2$. In a theoretical simulation of the spectrum,[4,33] the wave functions of the ground Al(3p)−$o$$H_2$/$p$$D_2$ bend−stretch levels are expressed in the radial and angular nuclear ($R$,$\theta$) and electronic coordinates through a diabatic representation of the three PESs emanating from the Al(3p) + $H_2$ asymptote. In the case of a free ← bound transition in a diatomic molecule, e.g., AlNe, the width of the spectral feature depends on the spatial extent of the ground-state vibrational wave function and the slope of the excited-state potential energy curve.[30] The situation is more complicated for atom-molecule complexes because of the rotational motion of the diatom, and especially for a complex involving an open-shell atom such as B and Al. The dissociation energy for the Al(3p)−$p$$D_2$ complex is greater than that of Al(3p)−$o$$H_2$. This arises from the larger reduced mass of the former complex and hence smaller radial extent of the wave function of the ground bend−stretch level. By the Franck−Condon reflection principle,[30] this implies a narrower spread of the free ← bound spectral feature. A similar difference in widths was found for the free ← bound spectra of the isovalent 3s ← 2p transition in the B−$o$$H_2$ and B−$p$$D_2$ complexes.[4]

### 4. Fit of the AlNe($B\ ^2\Sigma^+$) Potential Energy Curve

Bound → free emission[34,35] and free ← bound excitation[24,36] spectra have been employed to derive potential energy curves for repulsive lower and upper states, respectively, of electronic transitions of weakly bound diatomic complexes. In this section, we derive the potential energy curve for the AlNe($B\ ^2\Sigma^+$) state, using the laser fluorescence excitation spectrum reported in section 3.2.1.

The intensity at excitation wavenumber $\sigma$ for excitation out of the ground $X_1\ ^2\Pi_{1/2}$ spin−orbit level can be expressed as[30,29]

$$I(\sigma) \propto |\langle B\Sigma, E|X\Pi_{1/2}, v'' = 0\rangle|^2 \qquad (4)$$

where $\langle B\Sigma, E\rangle$ is the upper-state continuum wave function and $|X\Pi_{1/2}, v'' = 0\rangle$ is the vibrational wave function of the lower state. The translational energy $E$ in the upper state equals $hc\sigma - hc\sigma(^2S - {}^2P_{1/2}) - D_0''$, where $\sigma(^2S - {}^2P_{1/2})$ is the transition wavenumber for the atomic line and $D_0''$ is the dissociation energy of the lower state. In previous work,[19] we obtained $D_0'' = 14.1 \pm 0.3$ cm$^{-1}$. The continuum wave function is energy normalized[37]

$$\lim_{R\to\infty} \langle B\Sigma, E\rangle = (2\mu_{AlNe}/\pi\hbar^2k^2)^{1/2} \sin(kR - l\pi/2 + \eta) \qquad (5)$$

where $k$ is the asymptotic wave vector, $\mu_{AlNe}$ is the Al−Ne reduced mass, $l$ is the orbital angular momentum (set equal to 0, because of the low beam rotational temperature), and $\eta$ is the phase shift. The $B - X$ electronic transition moment is assumed not to vary with $R$, as was found to be the case in ab initio calculations for the analogous $B\ ^2\Sigma^+ - X\ ^2\Pi$ transition in the BAr complex.[35]

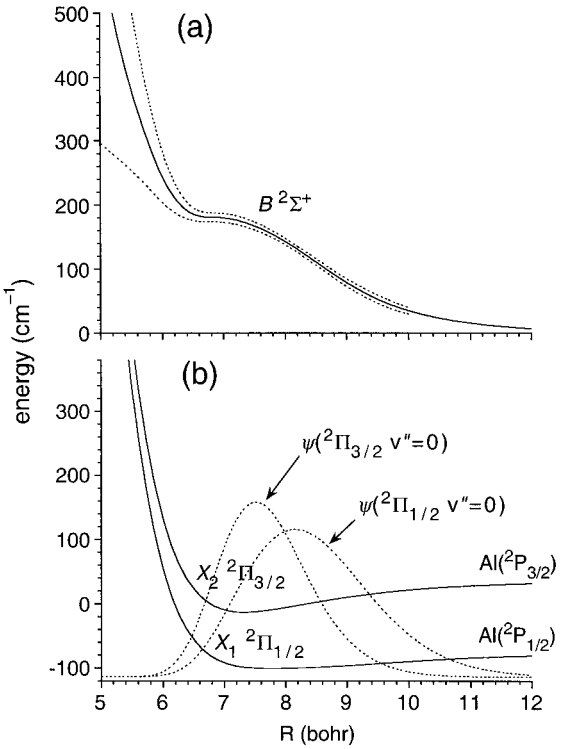


**Figure 8.** (a) The manually fit Al(4s)Ne $B\ ^2\Sigma^+$ state potential energy curve. The solid line denotes the best fit potential energy curve and the two dotted lines denote the estimated uncertainties in the interaction energies. (b) The computed (ref 19) potential energy curves for the Al(3p)-Ne $X\ ^2\Pi$ spin−orbit levels (solid lines) and the calculated $v'' = 0$ ground-state vibrational wave functions (dotted lines).

In using eq 4 to generate a simulated spectrum, the ground-state vibrational wave function was computed using a potential energy curve for the AlNe($X_1\ ^2\Pi_{1/2}$) spin−orbit level based on ab initio computed spin-free Al(3p)Ne $X\ ^2\Pi$ and $A\ ^2\Sigma^+$ potential energy curves.[19] Figure 8(b) displays the potential energy curve and the $v'' = 0$ vibrational wave function, obtained through solution of the 1-dimensional nuclear Schrödinger equation. We parametrize the excited-state $B\ ^2\Sigma^+$ potential energy curve by assuming values over a grid of $R$ covering the spatial region where the ground-state vibrational wave function has significant amplitude [$R$ = 5.9, 6.5, 6.9, 8.0, 9.0, 10.0 bohr] and extrapolating to larger and smaller $R$ values with exponential repulsive functions of the form $V_s \exp(-\alpha_s R)$. The values over the grid are varied until good agreement with the experimental spectrum is achieved. The inner and outer exponential scaling factors $\alpha_s$ were also adjusted.

In our previous spectroscopic study of the AlNe complex,[19] we found that there was a significant concentration of the $v'' = 0$ level of the spin−orbit excited $X_2\ ^2\Pi_{3/2}$ level, as well as the ground $X_1\ ^2\Pi_{1/2}\ v'' = 0$ level, in the beam for seed gas mixtures with high Ne mole fraction. Although the concentration of the excited spin−orbit level is not expected to be large under the presently employed beam conditions, we nevertheless included excitation out of the $X_2\ ^2\Pi_{3/2}$ level in our simulations

The adjustable parameters defining the excited-state potential energy curve were varied manually to fit the experimentally observed spectrum in Figure 6. Figure 8(a) presents the derived potential energy curve for the AlNe($B\ ^2\Sigma^+$) state, whereas Figure 8(b) presents the potential energy curves and the $v'' = 0$ vibrational wave functions for the lower $X\ ^2\Pi$ spin−orbit levels, for comparison. The solid line in Figure 8(a) denotes the estimated $B\ ^2\Sigma^+$ potential energy curve, while the upper and lower dotted lines denote its estimated uncertainty. Table 5

**TABLE 5: Parameters Defining the AlNe($B\ ^2\Sigma^+$) Potential Energy Curve**

| parameter[a] | value |
|---|---|
| $V(5.9)$ | 266 |
| $V(6.5)$ | 186 |
| $V(6.9)$ | 181 |
| $V(8.0)$ | 143 |
| $V(9.0)$ | 79 |
| $V(10.0)$ | 35 |
| $\alpha_s$ (inner) | 0.9 |
| $\alpha_s$ (outer) | 0.8 |

[a] $V(R)$ denotes the value (in $cm^{-1}$) of the potential energy at $R$ (in bohr), and the exponential scaling factors $\alpha_s$ are given in units of $bohr^{-1}$.

presents the values of the fitted parameters. The different radial ranges and widths of the $v'' = 0$ vibrational wave functions for the $X\ ^2\Pi$ spin−orbit levels reflects differences in the binding energies of these levels; this has been discussed in detail upon previously.[19]

The shape of the spectral feature is dictated primarily by the transition out of the ground $X_1\ ^2\Pi_{1/2}$ spin−orbit level. Our simulated spectrum, presented in Figure 6, reproduces the experimental spectrum very well, except for excitation wavenumbers close to that of the strong Al 4s $^2S_{1/2} \leftarrow$ 3p $^2P_{1/2}$ atomic line. We find that the reproducibly observed peak on the shoulder of the feature can be assigned as excitation out of the spin−orbit excited $X_2\ ^2\Pi_{3/2}$ level. The relative intensity of this peak implies that the $X_2\ ^2\Pi_{3/2}$ concentration in the beam is ∼7% of that of the ground spin−orbit level. This is not inconsistent with our observation[19] of nearly equal spin−orbit populations at high Ne mole fractions in the seed gas. We have no evidence for the presence of other spin−orbit excited complexes in our experiments.

The maximum intensity occurs at a transition wavenumber approximately equal to the difference in electronic energies at the internuclear separation corresponding to the peak of the lower-state vibrational wave function. From the asymmetry of the spectrum, we have inferred a potential energy curve with a broad shoulder similar in form to that of the potential energy curve for the isovalent BNe($B\ ^2\Sigma^+$) state.[24] This "shelf" in the AlNe($B\ ^2\Sigma^+$) system occurs at somewhat lower repulsive energies (∼200 $cm^{-1}$) and larger internuclear separations (∼7 bohr) as compared to the shelf for BNe($B\ ^2\Sigma^+$), which is computed[24] to lie ∼300 $cm^{-1}$ above the B(3s) + Ne asymptotic energy at $R \approx 6$ bohr. From the lack of sharp resonance features in the spectrum, the possible small well on the shoulder of the repulsive wall in the AlNe($B\ ^2\Sigma^+$) potential energy curve cannot support even one quasibound vibrational level.

The uncertainty in the derived potential energy curve is large for $R < 6$ bohr. The wave function amplitude for these small internuclear separations contributes most strongly to the blue end of the spectrum. Because the amplitude for this range of $R$ is small, the spectrum is not particularly sensitive to the potential at small $R$. Similarly, the potential at large $R$ is not well determined. The uncertainties plotted in Figure 8(a) for this range of $R$ are small because we have assumed a purely repulsive excited-state potential energy curve. In principle, there could be a small attractive well, to which our data are not sensitive. By contrast, the potential in the Franck−Condon region is well determined (±5 $cm^{-1}$).

## 5. Discussion

This paper has presented an exploration of the 4s ← 3p electronic transition in a number of van der Waals complexes involving the Al atom. The observed spectra reveal both attractive and repulsive interactions of the excited Al(4s) atom with the investigated atomic and molecular partners. We also present the 3d ← 3p transition in the Al−$N_2$ and Al−$CH_4$ complexes. Observation of this transition in AlNe and Al−$H_2$/$D_2$ has been reported previously.

From the free ← bound nature of the excitation spectra, we conclude that the excited-state PESs for AlNe and Al−$H_2$/$D_2$ are repulsive. In the case of AlNe, we were able to construct a potential energy curve for the excited $B\ ^2\Sigma^+$ electronic state by modeling the excitation spectrum. This potential energy curve is qualitatively similar to that of the isovalent BNe($B\ ^2\Sigma^+$) state, which correlates with the B(3s) + Ne asymptote, and possesses a "shelf" on the repulsive wall. The potential energy curves for both the BAr($B\ ^2\Sigma^+$) and AlAr($B\ ^2\Sigma^+$) electronic states[28,38−40] possess a barrier at large $R$ and an inner attractive well which supports a number of bound and quasibound vibrational levels. In a review of the work on metal−rare gas complexes, Breckenridge[41] noted that such barriers should be a general feature of electronic states of these complexes correlating with metal atom ns Rydberg states. The barrier is ascribed to Fermi repulsion of the rare gas by the diffuse metal ns orbital. The polarizability of Ne is less than that of Ar, and the shoulders found on the repulsive potential energy curves for BNe($B\ ^2\Sigma^+$) and AlNe($B\ ^2\Sigma^+$) electronic states are a residue of the short-range attractive well behind a long-range barrier seen in the BAr($B\ ^2\Sigma^+$) and AlAr($B\ ^2\Sigma^+$) states.

In similar fashion, the 4s electronic state of the Al−$H_2$/$D_2$ complex has been found to be repulsive in the Franck−Condon region in optical excitation from the ground 3p bend−stretch level, as was previously found[4] for the 3s state of the isovalent B−$H_2$/$D_2$ complex. Although a simulation of our spectra for these isotopomeric complexes awaits the availability of the Al(4s)−$H_2$ PES, we estimate that the energy of this state, at the ground-state equilibrium geometry [Al−$H_2$ separation $R = 5.80$ bohr], is approximately 390 $cm^{-1}$ greater than that of the Al(4s) + $H_2$ asymptote. The repulsive energy of the B(3s)−$H_2$ state in the Franck−Condon region is ∼580 $cm^{-1}$,[4,33] somewhat greater than in the Al(4s)-$H_2$ system. To judge by the blue shifts of the 4s ← 3p transitions in the spectra of the AlNe and Al−$H_2$/$D_2$ complexes (see Figures 6 and 7), the Al(4s)−$H_2$ excited state is more repulsive than the AlNe($B\ ^2\Sigma^+$) state. This is exactly analogous to what we previously found for the corresponding B(3s)−$H_2$ and BNe($B\ ^2\Sigma^+$) excited states.[4,24]

In contrast to the repulsive character of the electronic states of AlNe and Al−$H_2$/$D_2$ correlating with the Al(4s) asymptote, the higher 5s states of these complexes are bound.[9,19] The Al 4d atomic state lies only 1200 $cm^{-1}$ higher than the 5s state, and the attractive nature of these states can be explained by mixing[9] of the atomic states induced by the approach of the atomic or molecular partner

As in the case of the complexes of the Al atom with the heavier rare gases (Ar, Kr and Xe),[28,40,42,43] the PES of the 4s excited states of the Al−$N_2$ and Al−$CH_4$ complexes have been found to be attractive. Lower bounds to the dissociation energies for these electronic states have been estimated in this study. These dissociation energies are significantly less than the values for electronic states derived from the higher 5s and 4d atomic states (see table 3 of ref [8]). Similarly, the dissociation energies of the AlAr and AlKr $B\ ^2\Sigma^+$ states, which correlate with the Al(4s) atomic state, are smaller than the dissociation energies[28] of higher ns Rydberg states and the $^2\Delta$ and $^2\Pi$ electronic states associated with Al nd atomic states.

It is interesting to consider the implications of these results for the interpretation of the spectra of Al atom doped solid

hydrogen. Krumrine et al.[3] investigated the equilibrium properties of an atomic boron impurity in solid *p*-$H_2$ through path-integral molecular dynamics calculations. The 3s ← 2p electronic transition was also simulated. These calculations were carried out with ab initio PESs[32,33] which take into account the anisotropic nature of the singly filled 2p orbital and which were calibrated by comparison with fluorescence excitation spectra of the binary B−$H_2$ complex taken in our laboratory.[4]

The B atomic 3s ← 2p transition, which occurs at 249.8 nm in the isolated atom, was predicted[3] to be shifted to the blue by approximately 6000 $cm^{-1}$ for B-atom doped solid p−$H_2$. The predicted shifts were slightly different for site-substituted and defect solids. In the site-substituted doped solid, the B atom is surrounded by 12 nearest-neighbor hydrogen molecules. The distance between the B atom and a nearest-neighbor $H_2$ is similar to that in the binary B−$H_2$ complex. The 6000 $cm^{-1}$ blue shift can be qualitatively explained as the result of the additive shift of ∼500 $cm^{-1}$ from each binary interaction with the nearest-neighbor $H_2$ molecules.

The experimental absorption spectrum for B-atom doped solid p−$H_2$ for wavelengths greater than 200 nm was found to exhibit two peaks, at 216.6 and 208.9 nm.[2] From the agreement of the observed wavelength with that for the simulated[3] 3s ← 2p transition, the former peak is assigned to this transition. There is a second electric-dipole allowed transition in atomic boron for wavelengths > 200 nm, namely the $2s2p^2\ ^2D \leftarrow 2s^22p\ ^2P$ transition at 208.9 nm.[44] The shorter-wavelength peak in the absorption spectrum of B-atom solid p−$H_2$ is assigned[2,3] to this transition, as the centroid of the transition to this state in the binary B−$H_2$ complex is not found to be strongly shifted[5] from the wavelength of this transition in the free atom.

The first absorption feature appears at 330 nm for Al-atom doped solid p−$H_2$.[1,45] This is considerably to the blue of the longest wavelength transition, $4s\ ^2S_{1/2} \leftarrow 3p\ ^2P_{1/2}$ at 394.4 nm, and slightly to the red of the next transition, $3d\ ^2D_{3/2} \leftarrow 3p\ ^2P_{1/2}$ at 308.2 nm, in the free Al atom[46] From the free ← bound nature of the 4s ← 3p transition in the binary Al−$H_2$ complex, as in the isovalent B−$H_2$ complex, we infer that this transition would be blue shifted in Al-atom doped solid p−$H_2$. Taking the derived 390 $cm^{-1}$ repulsive energy for the binary Al(4s)-$H_2$ complex at the equilibrium geometry of the ground electronic state, we estimate that the interaction of the atom with the 12 nearest-neighbor hydrogen molecules in the doped solid would shift the 4s ← 3p transition to 333 nm. This is very close to the observed wavelength[1,45] for this transition in Al-doped solid hydrogen. It would be desirable to carry out a full simulation of the transition, to obtain a more accurate estimate of the wavelength and shape of the transition in the doped solid.

In previous work,[9] we observed the bands of the binary Al−$H_2$ complex corresponding to the 3d ← 3p electronic transition. Radial cuts in $C_{2v}$ geometry were also computed for the 5 PESs emanating from the Al(3d) + $H_2$ asymptote. From both the experimental spectra and the ab initio calculations,[9] the upper levels of these transitions were found to be attractive. This suggests that 3d ← 3p transition is red shifted in the doped solid. For the purpose of estimating the oscillator strength of the transition in the doped solid which peaks at 330 nm, it thus seems reasonable to surmise that this peak encompasses the overlapped 4s ← 3p and 3d ← 3p transitions.

**Acknowledgment.** This research was supported by the U.S. Air Force Office of Scientific Research (AFOSR) under grant no. F49620-01-1-0183. We greatly appreciate the support and encouragement of Millard Alexander.

## References and Notes

(1) Fajardo, M. E.; Tam, S.; Thompson, T. L.; Cordonnier, M. E. *Chem. Phys.* **1994**, *189*, 351.
(2) Tam, S.; Macler, M.; DeRose, M. E.; Fajardo, M. E. *J. Chem. Phys.* **2000**, *113*, 9067.
(3) Krumrine, J. R.; Jang, S.; Alexander, M. H.; Voth, G. A. *J. Chem. Phys.* **2000**, *113*, 9079.
(4) Yang, X.; Hwang, E.; Alexander, M. H.; Dagdigian, P. J. *J. Chem. Phys.* **1995**, *103*, 7966.
(5) Yang, X.; Dagdigian, P. J. *Faraday Discuss.* **1997**, *108*, 287.
(6) Yang, X.; Dagdigian, P. J. *J. Chem. Phys.* **1998**, *109*, 8920.
(7) Yang, X.; Gerasimov, I.; Dagdigian, P. J. *Chem. Phys.* **1998**, *239*, 207.
(8) Gerasimov, I.; Lei, J.; Dagdigian, P. J. *J. Phys. Chem. A* **1999**, *103*, 5910.
(9) Tan, X.; Dagdigian, P. J.; Alexander, M. H. *Faraday Discuss.* **2001**, *118*, 387.
(10) Tan, X.; Dagdigian, P. J.; Williams, J.; Alexander, M. H. *J. Chem. Phys.* **2001**, *114*, 8938.
(11) Dagdigian, P. J.; Yang, X.; Gerasimov, I.; Lei, J. In *Atomic and Molecular Beams: The State of the Art 2000*; Campargue, R., Ed.; Springer: Berlin, 2001; p 367.
(12) Brock, L. R.; Duncan, M. A. *J. Phys. Chem.* **1995**, *99*, 16 571.
(13) Jakubek, Z. J.; Simard, B. *J. Chem. Phys.* **2000**, *112*, 1733.
(14) Pilgrim, J. S.; Robbins, D. L.; Duncan, M. A. *Chem. Phys. Lett.* **1993**, *202*, 203.
(15) Agreiter, J. K.; Knight, A. M.; Duncan, M. A. *Chem. Phys. Lett.* **1999**, *313*, 162.
(16) Yang, D.-S.; Miyawaki, J. *Chem. Phys. Lett.* **1999**, *313*, 514.
(17) Greetham, G. M.; Hanton, M. J.; Ellis, A. M. *Phys. Chem. Chem. Phys.* **1999**, *1*, 2709.
(18) Reho, J. H.; Merker, U.; Radcliff, M. R.; Lehmann, K. K.; Scoles, G. *J. Phys. Chem. A* **2000**, *104*, 3620.
(19) Yang, X.; Dagdigian, P. J.; Alexander, M. H. *J. Chem. Phys.* **1998**, *108*, 3522.
(20) Basinger, W. H.; Lawrence, W. G.; Heaven, M. C. *J. Chem. Phys.* **1995**, *103*, 7218.
(21) Loomis, R. A.; Schwartz, R. L.; Lester, M. I. *J. Chem. Phys.* **1996**, *104*, 6984.
(22) Yang, X.; Hwang, E.; Dagdigian, P. J. *J. Chem. Phys.* **1996**, *104*, 8165.
(23) Yang, X.; Dagdigian, P. *J. Chem. Phys.* **1997**, *106*, 6596.
(24) Yang, X.; Hwang, E.; Dagdigian, P. J.; Yang, M.; Alexander, M. H. *J. Chem. Phys.* **1995**, *103*, 2779.
(25) Chaban, G.; Gordon, M. S. *J. Chem. Phys.* **1997**, *107*, 2160.
(26) Halkier, A.; Coriani, S.; Jorgensen, P. *Chem. Phys. Lett.* **1998**, *294*, 292.
(27) Buckingham, A. D. *Adv. Chem. Phys.* **1967**, *12*, 107.
(28) Heidecke, S. A.; Fu, Z.; Colt, J. R.; Morse, M. D. *J. Chem. Phys.* **1992**, *97*, 1692.
(29) Tellinghuisen, J. *Adv. Chem. Phys.* **1985**, *60*, 299.
(30) Schinke, R. *Photodissociation Dynamics*; Cambridge U. P.: Cambridge, 1993.
(31) Hwang, E.; Dagdigian, P. J. *J. Chem. Phys.* **1995**, *102*, 2426.
(32) Williams, J.; Alexander, M. H. *J. Chem. Phys.* **2000**, *112*, 5722.
(33) Alexander, M. H.; Yang, M. *J. Chem. Phys.* **1995**, *103*, 7956.
(34) Fawzy, W. M.; Le Roy, R. J.; Simard, B.; Niki, H.; Hackett, P. A. *J. Chem. Phys.* **1993**, *98*, 140.
(35) Hwang, E.; Dagdigian, P. J.; Alexander, M. H. *Can. J. Chem.* **1994**, *72*, 821.
(36) Okunishi, M.; Yamanouchi, K.; Onda, K.; Tsuchiya, S. *J. Chem. Phys.* **1993**, *98*, 2675.
(37) Child, M. S. In *Specialist Periodical Reports: Molecular Spectroscopy*; The Chemical Society: London, 1974; p 466.
(38) Hwang, E.; Huang, Y.-L.; Dagdigian, P. J.; Alexander, M. H. *J. Chem. Phys.* **1993**, *98*, 8484.
(39) Alexander, M. H.; Walton, A. R.; Yang, M.; Yang, X.; Hwang, E.; Dagdigian, P. J. *J. Chem. Phys.* **1997**, *106*, 6320.
(40) McQuaid, M. J.; Gole, J. L.; Heaven, M. C. *J. Chem. Phys.* **1990**, *92*, 2733.
(41) Breckenridge, W. H.; Jouvet, C.; Soep, B. In *Advances in Metal and Semiconductor Clusters*; Duncan, M. A., Ed.; JAI Press: Greenwich, 1995; Vol. 3; p 1.
(42) Callender, C. L.; Mitchell, S. A.; Hackett, P. A. *J. Chem. Phys.* **1989**, *90*, 5252.
(43) Fu, Z.; Massick, S.; Kaup, J. G.; Benoist d'Azy, O.; Breckenridge, W. H. *J. Chem. Phys.* **1992**, *97*, 1683.
(44) Odintzova, G. A.; Striganov, A. R. *J. Phys. Chem. Ref. Data* **1979**, *8*, 63.
(45) Fajardo, M., private communication.
(46) Moore, C. E. *Atomic Energy Levels, NSRDS−NBS 35*; U. S. Government Printing Office: Washington, 1971; Vol. 1.